Electron Scattering at Steps: Image-Potential States on Cu(119)

Manfred Roth, Martin Pickel, Wang Jinxiong, Martin Weinelt,* and Thomas Fauster
Lehrstuhl für Festkörperphysik, Universität Erlangen-Nürnberg, Staudtstrasse 7, D-91058 Erlangen, Germany
(Received 17 October 2001; published 13 February 2002)

The dynamics of image-potential states on Cu(119) have been studied with two-photon photoemission. Direction-dependent quasielastic scattering processes with large momentum transfer are attributed to the finite terrace-width distribution on the stepped surface. This effectively couples image-potential states via interband scattering and leads to an asymmetry of the decay rate. Electrons in the first image-potential state live apparently longer when running upstairs.

DOI: 10.1103/PhysRevLett.88.096802 PACS numbers: 73.20.At, 79.60.Bm, 79.60.Dp, 79.60.Ht

Photoinduced surface reactions are usually driven by hot electrons which transiently attach to adsorbate levels [1]. A primary step towards a microscopic understanding of this dynamical process [2] is the study of photoexcited electrons at metal surfaces [3]. On an ideal surface the excited electron will loose its energy via inelastic scattering by bulk and surface electrons [4]. A real surface encloses, however, relaxation centers such as the transient products of the photochemical reaction itself or even simpler intrinsic point defects and steps. Such potential barriers provoke distinct electron scattering processes [5] which are sensitively probed by surface states [6].

On metal surfaces the dynamics of image-potential states [7] can be studied with femtosecond time resolution [8] by two-photon photoemission (2PPE) [9]. An electron excited by a first laser pulse is trapped at the distance of a few angstroms in front of the surface. The weak coupling to bulk states leads to lifetimes τ of tens of femtoseconds [7,8] and allows one to sample the evolution of the population by a second time-delayed probe pulse. During its lifetime the excited electron is subject to a variety of surface-specific scattering processes. Inelastic decay rates ($\Gamma = \hbar/\tau$) and quasielastic scattering rates increase with defect density. The branching ratio depends on the particular type of scattering potential [10] and on surface order [11]. While experiments so far proved the importance of surface-related decay channels, they did not provide a microscopic model of the scattering process itself. Recently, such a quasielastic relaxation channel was observed, which couples image-potential states with a different quantum number n [12]. The actual origin of the scattering process remained, however, unconcealed.

In this Letter we address scattering processes at steps in the lateral superlattice of Cu(119) (see Fig. 1 top). The 2PPE experiment [13] used the fundamental ($h\nu = 1.53$ eV, pulse width 35 fs) and frequency-tripled ($3h\nu = 4.59$ eV, 63 fs) radiation from a Ti:sapphire oscillator as probe and pump pulse, respectively. The pump photon energy was chosen close to the work function $\Phi = 4.60$ eV, so that intermediate states up to the vacuum level E_{vac} were accessible. Electrons were detected after a hemispherical energy analyzer with an energy and angular resolution of 30 meV and $\pm 1.5°$, respectively. Sample preparation followed standard procedures for Cu [10]. Sample cleanliness was controlled by x-ray photoelectron spectroscopy, step order by low-energy electron diffraction. Measurements were performed at a base pressure of 2×10^{-11} mbar with the sample kept at room temperature.

As for Cu(001) [8] we find on the vicinal Cu(119) surface a series of image-potential states (see bottom spectra of Fig. 3). The first three members $n = 1, 2, 3$ can be resolved in the energy domain which allows one to map the band dispersion $E(k_\parallel)$ depicted in Fig. 1 (filled circles). The lateral superlattice manifests itself by umklapp processes of the $n = 1$ and 2 image-potential-state bands [14]. The dispersion parallel to the step edge equals the one of a flat surface. Thus the image-potential states react to the step potential in the way expected for Bloch states, i.e., $E(k_\parallel) = E(k_\parallel + G_\parallel)$, where $G_\parallel = 2\pi/11.6$ Å $= 0.54$ Å^{-1} is a reciprocal lattice vector of the (119) superlattice. The periodicity confirms that $k_\parallel$ is conserved with respect to the average

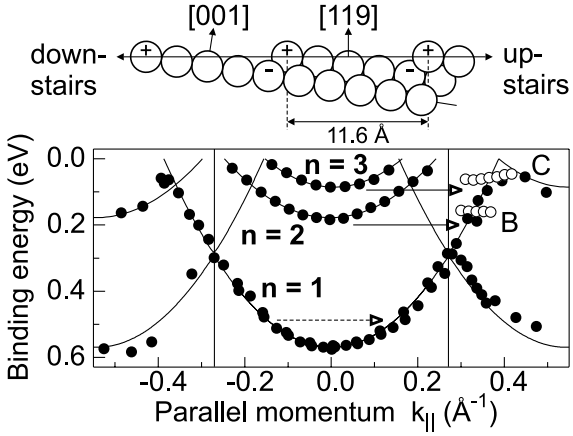

FIG. 1. Top: Hard-sphere model of bulk truncated Cu(119) as projected on the $(1\bar{1}0)$ plane. Bottom: Energy vs in-plane momentum dispersion curves $E(k_\parallel)$ for Cu(119). Positive (negative) $k_\parallel$ values correspond to the direction running upstairs (downstairs) perpendicular to the steps. The surface Brillouin zone boundary is indicated by vertical lines.

 0031-9007/02/88(9)/096802(4)$20.00

surface plane and indicates a coherent wave function of the image-potential states extending over several terraces, i.e., negligible localization [13].

In Table I decay rates Γ_n at the band bottom E_n^0 are compared for Cu(001) and Cu(119). The decrease of the decay rate with increasing quantum number n can be rationalized by the reduced bulk penetration $\propto n^{-3}$ [7]. The overall larger decay rate on the stepped surface is attributed to a narrowing of the Cu(001) gap near the X point when projected along the [119] direction [13]. This leads to an increase of unoccupied bulk states serving as decay channels in inelastic electron-electron scattering.

Studying the momentum dependence of the decay rate we note that at smaller binding energy the phase space of unoccupied states increases further and we expect the decay rate to grow. This behavior is observed for Cu(001) where decay into bulk states and along the image-potential-state parabola itself lead to a linear increase of the decay rate [15]. As seen from Fig. 2 the dynamics on Cu(119) are more intricate. While for the $n = 2$ image-potential state the $k_\parallel$ dependence of the decay rate is symmetric and roughly parabolic, it depends on direction for $n = 1$: Electrons running upstairs apparently live longer than those running downstairs. This asymmetry and, in particular, the decrease of the decay rate for positive momenta cannot be related to band-structure effects. Inelastic bulk and intraband decay channels are independent of direction $[E(k_\parallel) = E(-k_\parallel)]$. Thus the distinct decay rates $\Gamma_1(k_\parallel) \neq \Gamma_1(-k_\parallel)$ point to a direction-dependent quasielastic scattering process and we clarify its nature in the rest of this Letter.

Figure 3 depicts sets of energy-resolved spectra close to the surface Brillouin zone (SBZ) boundary (emission angle $\approx 28°$) for positive $k_\parallel$ values. Each set contains from top to bottom spectra measured at increasing pump-probe delay T_d. For $T_d = 35$ fs spectra are dominated by the $n = 1$ image-potential state and we resolve the lower and the upper branch (LB and UB) of the $n = 1$ band in the second SBZ. Spectra change considerably for increased pump-probe delay. The LB signal of the $n = 1$ image-potential state depends on direction. Emission intensity in the first SBZ (26°) persists significantly longer than in the second SBZ (38°). Noting $E(k_\parallel) = E(k_\parallel - G_\parallel)$ this corroborates that electrons running upstairs live apparently longer than those running downstairs.

TABLE I. Binding energies E_n^0 [13] and decay rates Γ_n for image-potential states on Cu(001) and Cu(119) at $k_\parallel = 0$. Error for energy values is ± 10 meV.

	Cu(001), $\Phi = 4.63$ eV		Cu(119), $\Phi = 4.60$ eV	
n	E_n^0 (meV)	Γ_n (meV)	E_n^0 (meV)	Γ_n (meV)
1	590	19 ± 3	556	44 ± 15
2	180	5.5 ± 0.7	176	17 ± 2.3
3	85	2.2 ± 0.15	84	7 ± 1
4	50	1.05 ± 0.1	48	3.5 ± 0.4

Two new, obviously long-lived components marked B and C become visible for $T_d \geq 70$ fs. Respective peak positions are indicated in Fig. 1 as open circles. The binding energy of peaks B and C is ≈ 40 meV smaller than at the bottom of the $n = 2$ and 3 image-potential-state bands and maximum intensity is observed when the momentum coincides with the parabola of the $n = 1$ band. In contrast to the dispersing $n = 1$ band, peak B stays at constant energy. With increasing pump-probe delay the intensity of peak C outweighs that of peak B.

To determine the respective decay rates we follow the upper branch of the $n = 1$ image-potential-state band in the second SBZ and record the signal as a function of delay between pump and probe pulses for $k_\parallel$ running upstairs. Data are shown after background subtraction on a semilogarithmic scale in Fig. 4a (solid circles). Depending on the binding energy the signal contains three components (I, II, and III). To evaluate their decay rates and percentages depicted in Fig. 4b, spectra have been decomposed into three exponential decaying contributions. For binding energies larger than 300 meV, spectra mainly trace the decay of the $n = 1$ image-potential state after direct population by the pump pulse. The onset of component II can be described quite well by a Gaussian centered at $E_2^0 - 80$ meV with a maximum contribution of $\approx 80\%$ and a width of 125 meV. The decay rate $\Gamma_{II} \approx 19$ meV is only slightly larger than that of the $n = 2$ image-potential state near $k_\parallel = 0$. This suggests that component II and thereby peak B stem from electrons originally excited to the $n = 2$ band and subsequently scattered to states on the $n = 1$ image-potential-state parabola. For somewhat smaller binding energies the contribution $|2\rangle \rightarrow |1\rangle$ levels off as seen from both energy- and time-resolved spectra. This behavior is understood realizing that the decay rate of the $n = 2$ image-potential state increases with parallel momentum (Fig. 2) and that electrons will cumulate at the $n = 2$ band bottom due to intraband scattering [15]. The peaklike shape of

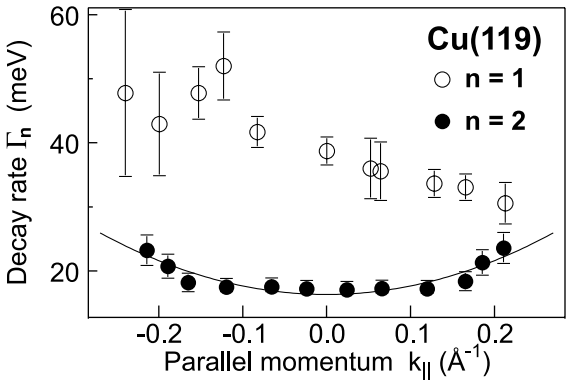

FIG. 2. Decay rate for $n = 1$ and 2 image-potential states as a function of parallel momentum. $k_\parallel > 0$ corresponds to the direction running upstairs. The errors indicate the relative uncertainties within the series of measurements. For absolute errors, see Table I.

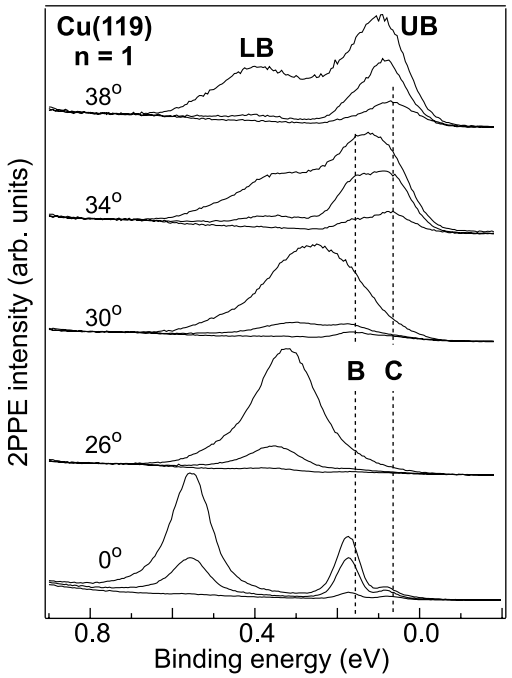

FIG. 3. Sets of angle- and energy-resolved spectra for Cu(119) for emission angles close to the SBZ edge (≈28°). Each set contains from top to bottom three spectra measured at increasing pump-probe delay of $T_d = 35, 70$, and 100 fs (125 fs for 34° and 38°). Intensity above $E_{\text{vac}} = 0$ is close to zero in all spectra.

B implies that interband scattering involves negligible energy transfer. Therefore one would naively expect peak B at energy E_2^0. The observed upward shift is attributed to finite angular resolution. In first order approximation such a broadening vanishes for $\nabla E(k_\parallel) = 0$. This holds for $k_\parallel = 0$, i.e., at the band bottom. Because of interband scattering the population of the $n = 2$ band is, however, probed at $k_\parallel \neq 0$, where finite angular resolution leads to an asymmetric broadening and a shift of the maximum to binding energies smaller than E_2^0. This also explains the shape of curve II and the somewhat larger decay rate Γ_{II}. While interband scattering $|2\rangle \rightarrow |1\rangle$ starts at energy E_2^0, finite resolution broadens the onset and shifts the maximum to smaller binding energies. Tracing thereby states with binding energies $< E_2^0$ leads to decay rates $> \Gamma_2$.

Following the above discussion, contribution III and thereby peak C are ascribed to interband scattering $|n \geq 3\rangle \rightarrow |1\rangle$. The decrease of the decay rate Γ_{III} with decreasing binding energy is attributed to successively sampling higher states of the Rydberg-like series via interband scattering when moving up the $n = 1$ band. This also explains the slight shift of peak C to smaller binding energies with increasing $k_\parallel$ (see Fig. 1). For energies close to E_{vac} quantum beats [8] are seen in the time-resolved measurements of Fig. 4a. The period of 115 ± 5 fs equals $h/|E_3^0 - E_4^0|$ and stems thus from coherent excitation of the $n = 3$ and 4 image-potential states. This proves that interband transitions $|n\rangle \rightarrow |1\rangle$ occur predominantly close

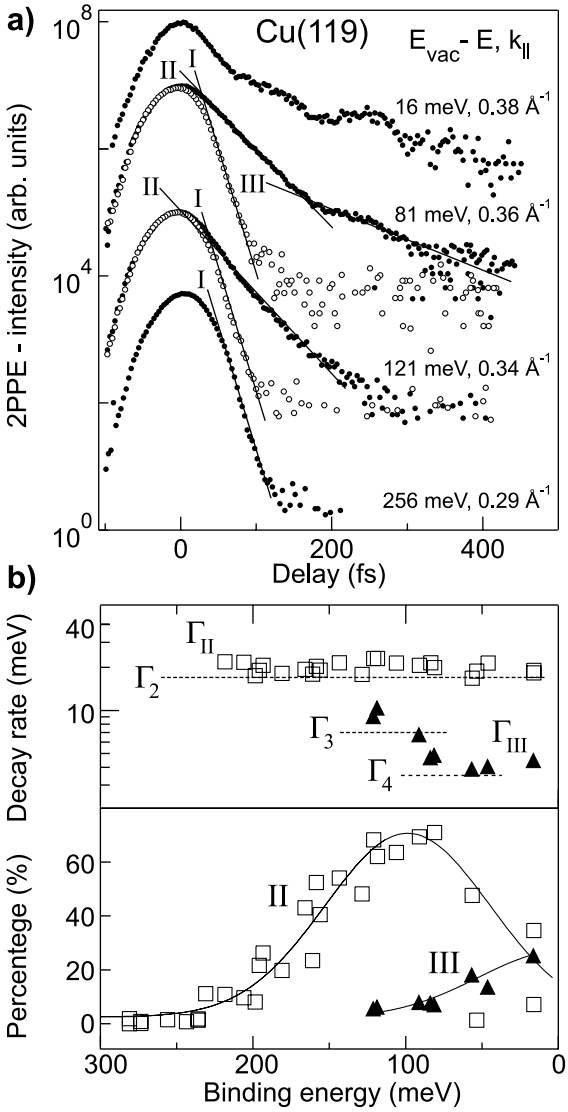

FIG. 4. (a) Time-resolved 2PPE measurements of the $n = 1$ image-potential state on Cu(119) as a function of binding energy plotted on a semilogarithmic scale. Spectra are recorded for $k_\parallel$ running upstairs (solid circles) and downstairs (open circles). Components I, II, and III are indicated by solid lines. (b) Decay rates and percentage of components II and III.

to the surface, where the $n = 1$ image potential has its maximum probability density and the oscillatory motion of the electron perpendicular to the surface [8] is probed.

As mentioned in the introduction interband scattering has been observed for clean Cu(001) and it was argued that the process is caused by point defects on the albeit flat surface [12]. Point defects are certainly present on any surface and provoke quasielastic scattering [10]. Nevertheless, on Cu(119) interband scattering has a different origin. This is immediately seen from time-resolved measurements recorded for $k_\parallel$ running downstairs (open circles in Fig. 4a) where components II and III are hardly observable (≤6%). This sizable asymmetry proves that interband scattering is indeed caused by steps. For a perfectly

ordered surface and neglecting phonon contributions [16] quasielastic scattering will not occur. Thus the origin of interband scattering has to be attributed to surface disorder, i.e., the finite terrace-width distribution on Cu(119). As indicated by the arrows in Fig. 1 momentum transfer in interband scattering is close to $G/2$ which corresponds in real space to twice the step separation d of the superlattice. Irregularities in the step separation [17] will therefore provide the necessary momentum. The pronounced direction dependence of the interband scattering process is surprising. The dipole associated with the step edge (see Fig. 1 top) would lead to a net attraction of the electron towards the surface. Parallel to the surface the electron would be accelerated in the downstairs direction in contrast to the observation. Obviously a thorough understanding of the interband scattering processes asks for detailed modeling including a self-consistent image potential at the step.

Elastic interband scattering out of the higher image-potential states competes with inelastic decay. Since both elastic and inelastic scattering take place at the surface, decay rates of $n \geq 2$ image-potential states on Cu(119) still exhibit the same n dependence as those on Cu(001). Comparing decay rates of higher image-potential states with Γ_1 in Table I, we estimate that elastic scattering contributes at least 20% to the total decay rate.

As evident for the $n = 2$ band inelastic decay is independent of direction and this should likewise hold for the $n = 1$ state. Considering the sizable interband scattering rate $|2\rangle \rightarrow |1\rangle$ and the orthogonality of initial and final states $\langle 2 \,|\, 1\rangle = 0$, we expect intraband scattering $|1, -k_{\|}\rangle \rightarrow |1, k_{\|}\rangle$ (dashed arrow in Fig. 1) to be much more likely. In this case the direction dependence in the scattering process leads to a redistribution of electrons on the image-potential-state parabola. States with momentum running upstairs become populated at the cost of states with momentum running downstairs. We therefore propose that the direction dependence of the decay rate of the $n = 1$ image-potential state is caused by the asymmetry in elastic scattering.

In the presence of defects new scattering pathways open, which strongly alter the dynamics of excited electrons. On Cu(119) the rather simple step-induced superlattice allows one to follow these processes in great detail. This demonstrates that elastic scattering at defects is a highly efficient relaxation channel which involves large momentum transfer and may be strongly direction dependent. Such processes can be of general importance in photochemistry when hot bulk electrons with finite momentum elastically tunnel into localized adsorbate resonances and drive the reaction at the surface.

We thank W. Berthold and U. Höfer for valuable discussions and preprints of their work. Support by the Deutsche Forschungsgemeinschaft is gratefully acknowledged.

*Electronic address: weinelt@physik.uni-erlangen.de

[1] *Laser Spectroscopy and Photochemistry on Metal Surfaces,* edited by H.-L. Dai and W. Ho (World Scientific, Singapore, 1995).
[2] M. Bonn *et al.,* Science **285**, 1042 (1999).
[3] C. Keller *et al.,* Phys. Rev. Lett. **80**, 1774 (1998); N.-H. Ge *et al.,* Science **279**, 202 (1998); A. Hotzel *et al.,* Chem. Phys. Lett. **285**, 271 (1998).
[4] H. Petek and S. Ogawa, Prog. Surf. Sci. **56**, 239 (1997); P. M. Echenique *et al.,* Chem. Phys. **251**, 1 (2000); I. Campillo *et al.,* Phys. Rev. Lett. **85**, 3241 (2000).
[5] G. Hörmandinger and J. B. Pendry, Phys. Rev. B **50**, 18 607 (1994).
[6] E. J. Heller *et al.,* Nature (London) **369**, 464 (1994); L. Bürgi *et al.,* Phys. Rev. Lett. **82**, 4516 (1999).
[7] P. M. Echenique and J. B. Pendry, J. Phys. C **11**, 2065 (1978).
[8] U. Höfer *et al.,* Science **277**, 1480 (1997).
[9] Th. Fauster and W. Steinmann, in *Photonic Probes of Surfaces,* edited by P. Halevi (North-Holland, Amsterdam, 1995), p. 347.
[10] M. Weinelt *et al.,* Appl. Phys. B **68**, 377 (1999); Th. Fauster *et al.,* Chem. Phys. **251**, 111 (2000).
[11] Ch. Reuß *et al.,* Phys. Rev. Lett. **82**, 153 (1999).
[12] W. Berthold *et al.,* Appl. Phys. B **73**, 865 (2001).
[13] M. Roth *et al.* (to be published).
[14] X. Y. Wang *et al.,* Phys. Rev. B **53**, 15 738 (1996); X. Y. Wang, X. J. Shen, and R. M. Osgood, Jr., *ibid.* **56**, 7665 (1997).
[15] W. Berthold *et al.,* Phys. Rev. Lett. **88**, 056805 (2002).
[16] Measurements at 100 and 300 K yield within experimental error identical results.
[17] M. Giesen, Surf. Sci. **370**, 55 (1997).